Predicting the High-Pressure Phase Equilibria of Binary Mixtures of Perfluoro-*n*-alkanes + *n*-Alkanes Using the SAFT-VR Approach

Clare McCabe,[†] Amparo Galindo,[†,‡] Alejandro Gil-Villegas,[†,§] and George Jackson*[,†,‡]

Department of Chemistry, University of Sheffield, Sheffield S3 7HF, U.K., Department of Chemical Engineering, Imperial College, London SW7 6BY, U.K., and Instituto de Física, Universidad de Guanajuato, Apdo. Postal E-143, León 37150, Mexico

Received: May 20, 1998

The phase behavior of perfluoro-(*n*)-alkane + (*n*)-alkane binary mixtures is of particular interest given their unexpected large positive deviations from Raoult's law. Binary mixtures of perfluoromethane + (*n*)-alkanes from methane to heptane are studied here, illustrating the continuous change in phase behavior from type II to type III that these systems exhibit. Some symmetrical systems that display heteroazeotropy are also examined. Using the statistical associating fluid theory for potentials of variable attractive range (SAFT-VR),we predict the high-pressure phase diagram for each binary mixture studied. The perfluoro-*n*-alkane and *n*-alkane molecules are treated as attractive spherical segments tangentially bonded together to form chains. We use simple empirical relationships between the number of carbon atoms and the number of segments in each chain. The attractive interactions are included as a square-well potential of depth ϵ and range λ. The pure component parameters are obtained by fitting to experimental vapor pressure and saturated liquid density data from the triple to the critical point. These optimized parameters are rescaled by the respective experimental critical points and used to determine the critical lines and phase behavior of the mixtures. The critical lines predicted by SAFT-VR for the perfluoro-*n*-alkane + *n*-alkane mixtures are in excellent agreement with the experimental data and improve significantly the results obtained with the simpler SAFT-HS approach, where the attractive interactions are treated at the mean-field level. This is particularly gratifying as the unlike dispersion interaction between the perfluoroalkane and alkane segments is obtained from a single mixture (perfluorobutane + *n*-butane) and then transferred to the other systems.

1. Introduction

One could be forgiven for expecting that perfluoroalkanes would exhibit very similar physical and chemical properties to the alkanes. They are very similar in structure, the fluorine atoms simply replacing the hydrogen atoms in the alkane molecules. However, that is where the similarity ends, as they possess very different physical properties. Binary mixtures of perfluoroalkanes and alkanes are of particular interest as they show substantial deviations from ideality, with large positive excess functions and extensive regions of liquid−liquid immiscibility. As a result of their unusual properties and behavior a large amount of experimental work has been devoted to their study.

By the late 40s the regular solution theory proposed by Hildebrand and Scatchard[1] could explain the thermodynamic properties of most solutions of nonpolar mixtures at least qualitatively. It was therefore reasonably proposed by Scott,[2] on the basis of the limited data available, that perfluorocarbon solutions would be no exception, and that hydrocarbon fluorocarbon mixtures would be completely miscible in all proportions. In fact subsequent experimental data for symmetrical hydrocarbon + perfluorocarbon mixtures, published in the early 50s (see refs 3−5), showed that these systems display substantial regions of liquid−liquid immiscibility. Various attempts to account for this anomalous behavior followed, with attention being focused on the failure of the geometric-mean assumption that the unlike attractive interactions could be described as the geometric mean of the like interactions: Simons and Dunlap[5] proposed the idea of interpenetration between neighboring C−H groups giving an abnormally strong hydrocarbon−hydrocarbon interaction energy leading to the failure of the geometric combining rule; Hildebrand[6] suggested that the solubility parameters of the hydrocarbons be empirically increased in order to fit the data, while Simons and Dunlap[5,7] suggested further corrections to the regular solution theory to include the effect of volume changes that occur on mixing; Reed[8] proposed yet another modification of regular solution theory to take into account size and ionization potential differences between the two components and then in late 50s introduced an additional fitted parameter.[9]

Rowlinson[10] concluded from a review of the data available that the anomalous behavior displayed by the hydrocarbon and fluorocarbon solutions resulted from an unusually weak hydrocarbon−fluorocarbon attractive interaction. However, this could not be proved as it was impossible to distinguish between a failure in assumptions made in describing the intermolecular forces and a failure in the theory itself. In the early 70s Dantzler and Knobler[11] proposed a test of the geometric-mean rule for hydrocarbon−fluorocarbon mixtures, by obtaining data from the interaction virial coefficient B_{12}. The results strongly supported the view that the anomalous behavior of hydrocarbon−fluorocarbon systems was due to the failure of the geometric-mean rule. They discussed possible reasons for such a weak unlike interaction between the two components: noncentral

[†] University of Sheffield.
[‡] Imperial College.
[§] Universidad de Guanajuato.

S1089-5647(98)02331-1 CCC: $15.00
Published on Web 09/22/1998

forces, large ionization potential differences, and large size differences, concluding that the observed deviation from the geometric-mean prediction was most likely due to the latter. The fact is that despite further experimental and theoretical work on these systems we are still without a convincing explanation, although it is believed to lie in the highly polarizable nature of the fluorine atoms.

In this paper we examine the phase behavior of binary mixtures of perfluoromethane + *n*-alkanes from methane to heptane. This series is particularly interesting to study as it illustrates the continuity that exists between liquid−liquid and gas−liquid equilibria. Using the classification of Scott and van Konynenburg,[12,13] systems of perfluoromethane + *n*-alkane up to *n*-propane show type II phase behavior: a continuous gas−liquid critical line connects the critical points of the pure components, and at lower temperatures a second liquid−liquid critical line extends from the upper critical end point (UCEP) to higher pressures; the three-phase line (liquid−liquid−gas) extends from lower temperatures and pressures to the UCEP where it terminates. As the mutual miscibility of the two components decreases, the region of liquid−liquid immiscibility shifts to higher temperatures, until it eventually interacts with the gas−liquid critical line. At this point, type II phase behavior becomes type III phase behavior, where the liquid−liquid and gas−liquid critical lines are connected. This phase behavior is first observed for the perfluoromethane + *n*-butane mixture. In type III mixtures at low temperatures the two liquids are immiscible as indicated by the three-phase line running from low pressure and temperature to the UCEP; a short gas−liquid critical line extends from the UCEP to the gas−liquid critical point of the more volatile component; the second fluid-fluid critical line starts from the gas−liquid critical point of the less volatile component and can extend to higher pressures in a variety of ways (four types of behavior for this critical line are common[13]). We are only concerned with that shown by perfluoromethane + *n*-butane and higher alkanes,where the critical line passes through a temperature minimum before continuing to higher pressures eventually extending beyond the pure component critical point. This behavior is known as gas−gas immiscibility of the second kind.[13]

High-pressure experimental investigations of the perfluorocarbon + hydrocarbon systems began around the mid 70s.[14−16] These provided a more detailed picture of the phase behavior in such systems since earlier work had been limited to normal or low pressures. Jeschke and Schneider[14] investigated the perfluoromethane + propane and perfluoromethane + *n*-butane systems and observed the switch from type II to III phase behavior, but it was De Loos et al.[17] who investigated the *n*-butane system in detail at lower pressures. They compared their results with the calculations of Mendonça[16] and Deiters,[18] who predicted the type of phase behavior for a number of perfluoromethane + (*n*)-alkane mixtures, determining correctly the change from a liquid-liquid critical line for perfluoromethane + propane to gas−gas critical behavior of the second kind for the perfluoromethane + *n*-butane system.

We use the SAFT-VR approach[19,20] for a square-well chain model to predict the fluid phase equilibria of the perfluoro-(*n*)-alkane + (*n*)-alkane systems. A comparison with the results obtained from the simpler SAFT-HS approach,[21] where the attractive interactions are treated at the van der Waals level using a one-fluid treatment, will also be discussed.

2. Models and Theory

As in earlier work,[19,21−26] the alkane and perfluoroalkane molecules are both modeled with a simple united atom approach: *m* hard-spherical attractive segments of diameter σ tangentially bonded together to form chains. We use a simple empirical relationship between the number of carbon atoms in the molecule and the number of segments in the model chain obtained by fitting to the critical behavior of the homologous series. For the perfluoroalkanes (component 1), $m_1 = 0.37(C - 1) + 1$; hence, a value of $m_1 = 1$ corresponds to perfluoromethane, $m_1 = 1.37$ to perfluoroethane, $m_1 = 1.74$ to perfluoropropane etc. For the alkanes (component 2) $m_2 = (C - 1)/3 + 1$. The attractive interactions are described via a square-well potential of width λ and depth ϵ

$$u_{ij}(r) = \begin{cases} +\infty & \text{if } r < \sigma_{ij} \\ -\epsilon_{ij} & \text{if } \sigma_{ij} \le r < \lambda_{ij}\sigma_{ij} \\ 0 & \text{if } r \ge \lambda_{ij}\sigma_{ij} \end{cases} \quad (1)$$

where r is the distance between the two segments and σ_{ij} defines the contact distance between spherical cores.

In this paper we will only summarize the main expressions of the SAFT-VR theory for the square-well potential; the reader should consult refs 19 and 20 for details. The general equation for mixtures of chain molecules formed from hard-core segments with attractive interactions is given followed by the specific expressions for the system of current interest. The Helmholtz free energy A for an n-component mixture of chain molecules can be separated into the various contributions as

$$\frac{A}{NkT} = \frac{A^{\text{IDEAL}}}{NkT} + \frac{A^{\text{MONO.}}}{NkT} + \frac{A^{\text{CHAIN}}}{NkT} \quad (2)$$

where N is the total number of molecules, T is the temperature, and k is the Boltzmann constant. There is no need to include the association term[19,20] since we are dealing with a nonassociating system. The ideal contribution to the free energy is given by a sum over all species i in the mixture[27]

$$\frac{A^{\text{IDEAL}}}{NkT} = \sum_{i=1}^{n} x_i \ln \rho_i \Lambda_i^3 - 1$$

$$= x_1 \ln \rho_1 \Lambda_1^3 + x_2 \ln \rho_2 \Lambda_2^3 - 1 \quad (3)$$

where $x_i = N_i/N$ is the mole fraction, $\rho_i = N_i/V$ the molecular number density, N_i the number of molecules, Λ_i the thermal de Broglie wavelength of species i, and V is the volume of the system. We can express the monomer Helmholtz free energy by

$$\frac{A^{\text{MONO.}}}{NkT} = (\sum_{i=1} x_i m_i)\frac{A^{\text{M}}}{N_s kT}$$

$$= (\sum_{i=1} x_i m_i) a^{\text{M}}$$

$$= (x_1 m_1 + x_2 m_2) a^{\text{M}} \quad (4)$$

where m_i is the number of spherical segments of chain i.

Using the Barker and Henderson high-temperature perturbation theory[28] for mixtures with a hard-sphere reference system, the monomer free energy per segment of the mixture is obtained from the expansion

$$a^{\text{M}} = a^{\text{HS}} + \beta a_1 + \beta^2 a_2 \quad (5)$$

where $\beta = 1/kT$ and each term is now for a mixture of spherical segments. The expression of Boublík[29] and Mansoori et al.[30] for a multicomponent mixture of hard spheres is used for the reference hard-sphere term

$$a^{HS} = \frac{6}{\pi\rho_s}\left[\left(\frac{\zeta_2^3}{\zeta_3^2} - \zeta_0\right)\ln(1-\zeta_3) + \frac{3\zeta_1\zeta_2}{(1-\zeta_3)} + \frac{\zeta_2^3}{\zeta_3(1-\zeta_3)^2}\right] \tag{6}$$

where ρ_s is the total number density of spherical segments and ζ_l are the reduced densities defined by

$$\zeta_l = \frac{\pi\rho_s}{6}\left[\sum_{i=1}^{n} x_{s,i}\sigma_{ii}^l\right]$$

$$= \frac{\pi\rho_s}{6}[x_{s,1}\sigma_{11}^l + x_{s,2}\sigma_{22}^l] \tag{7}$$

Here σ_{ii} is the diameter of the spherical segments of chain i and $x_{s,i}$ is the mole fraction of segments of type i in the mixture.

The mean-attractive energy represented by the a_1 term is obtained from the sum of the partial terms corresponding to each type of pair interaction[19,20]

$$a_1 = \sum_{i=1}^{n}\sum_{j=1}^{n} x_{s,i}x_{s,j}a_1^{ij}$$

$$= x_{s,1}^2\, a_1^{11} + 2x_{s,1}x_{s,2}a_1^{12} + x_{s,2}^2\, a_1^{22} \tag{8}$$

where

$$a_1^{ij} = -2\pi\rho_s\epsilon_{ij}\int_{\sigma_{ij}}^{\infty} r_{ij}^2\, g_{ij}^{HS}[r_{ij};\, \zeta_3]\, dr_{ij} \tag{9}$$

and g_{ij}^{HS} is the radial distribution function for a mixture of hard spheres. Using the mean value theorem,[19,20] we obtain an expression for a_1 in terms of the contact value of g_{ij}^{HS}

$$a_1 = -\rho_s\sum_i\sum_j x_{s,i}x_{s,j}\alpha_{ij}^{VDW}\, g_{ij}^{HS}[\sigma_{ij};\, \zeta_3^{eff}] \tag{10}$$

where

$$\alpha_{ij}^{VDW} = 2\pi\epsilon_{ij}\sigma_{ij}^3(\lambda_{ij}^3 - 1)/3 \tag{11}$$

is the van der Waals attractive constant for the $i-j$ interaction and ζ_3^{eff} is an effective packing fraction.

In the van der Waals one (VDW-1)-fluid theory g_{ij}^{HS} is approximated by the radial distribution function for a single fluid so that eq 10 simplifies to

$$a_1 = -\rho_s\sum_i\sum_j x_{s,i}x_{s,j}\alpha_{ij}^{VDW}\, g_0^{HS}[\sigma_x;\, \zeta_x^{eff}] \tag{12}$$

where g_0^{HS} is the contact value of the hard-sphere pair radial distribution obtained from the Carnahan and Starling equation of state[31]

$$g_0^{HS}[\sigma_x;\, \zeta_x^{eff}] = \frac{1 - \zeta_x^{eff}/2}{(1-\zeta_x^{eff})^3} \tag{13}$$

The effective packing fraction ζ_x^{eff} in eq 13 is obtained within the VDW-1 fluid approximation from the corresponding packing fraction of the mixture ζ_x

$$\zeta_x^{eff}(\zeta_x, \lambda_{ij}) = c_1(\lambda_{ij})\zeta_x + c_2(\lambda_{ij})\zeta_x^2 + c_3(\lambda_{ij})\zeta_x^3 \tag{14}$$

where

$$\zeta_x = \frac{\pi}{6}\rho_s\sum_i\sum_j x_{s,i}x_{s,j}\sigma_{ij}^3$$

$$= \frac{\pi}{6}\rho_s\sigma_x^3 \tag{15}$$

with

$$\sigma_x^3 = \sum_i\sum_j x_{s,i}x_{s,j}\sigma_{ij}^3 \tag{16}$$

The coefficients c_1, c_2, and c_3 are approximated by those of the pure fluid[19,20]

$$\begin{pmatrix} c_1 \\ c_2 \\ c_3 \end{pmatrix} = \begin{pmatrix} 2.25855 & -1.50349 & 0.249434 \\ -0.669270 & 1.40049 & -0.827739 \\ 10.1576 & -15.0427 & 5.30827 \end{pmatrix}\begin{pmatrix} 1 \\ \lambda \\ \lambda^2 \end{pmatrix} \tag{17}$$

This corresponds to the MX1b mixing rule of ref 20. The MX1b prescription gives an excellent representation of both vapor−liquid and liquid−liquid critical behavior.[26] If the actual packing fraction ζ_3 of the system is used in order to get ζ_3^{eff} according to the mapping rule for pure components (MX3b mixing rule in ref 20), there are some problems associated with the critical region of the phase diagram. This is a common feature of equations of state for mixtures that use parameters defined for pure fluids beyond the VDW-1 fluid approximation.[13,32]

The first fluctuation term a_2 is given by[19,20]

$$a_2 = \sum_{i=1}^{n}\sum_{j=1}^{n} x_{s,i}x_{s,j}a_2^{ij}$$

$$= x_{s,1}^2\, a_2^{11} + 2x_{s,1}x_{s,2}a_2^{12} + x_{s,2}^2\, a_2^{22} \tag{18}$$

The terms a_2^{ij} are obtained from the expressions for a_1^{ij} with the local compressibility approximation

$$a_2^{ij} = \frac{1}{2}K^{HS}\epsilon_{ij}\rho_s\frac{\partial a_1^{ij}}{\partial\rho_s} \tag{19}$$

where K^{HS} is the hard-sphere isothermal compressibility of Percus-Yevick

$$K^{HS} = \frac{\zeta_0(1-\zeta_3)^4}{\zeta_0(1-\zeta_3)^2 + 6\zeta_1\zeta_2(1-\zeta_3) + 9\zeta_2^3} \tag{20}$$

Finally, the contribution to the free energy due to chain formation is expressed in terms of the contact value of the background correlation function[19,20]

$$\frac{A^{CHAIN}}{NkT} = -\sum_{i=1}^{n} x_i(m_i - 1)\ln y_{ii}^{SW}(\sigma_{ii})$$

$$= -x_1(m_1 - 1)\ln y_{11}^{SW}(\sigma_{11}) - x_2(m_2 - 1)\ln y_{22}^{SW}(\sigma_{22}) \tag{21}$$

where $y_{ii}^{SW}(\sigma_{ii}) = g_{ii}^{SW}(\sigma_{ii})\exp(-\beta\epsilon_{ii})$. We obtain $y_{ii}^{SW}(\sigma_{ii})$ from the high-temperature expansion of $g_{ii}^{SW}(\sigma_{ii})$

$$g_{ii}^{SW}(\sigma_{ii}) = g_{ii}^{HS}(\sigma_{ii}) + \beta\epsilon_{ii}g_1(\sigma_{ii}) \tag{22}$$

The hard-sphere term g_{ii}^{HS} is given by the expression of Boublík[29]

$$g_{ij}^{HS}(\sigma_{ij};\zeta_3) = \frac{1}{1-\zeta_3} + 3\frac{D_{ij}\zeta_3}{(1-\zeta_3)^2} + 2\frac{(D_{ij}\zeta_3)^2}{(1-\zeta_3)^3} \quad (23)$$

with the parameter D_{ij} defined by

$$D_{ij} = \frac{\sigma_{ii}\sigma_{jj}}{\sigma_{ii}+\sigma_{jj}} \frac{\sum_{i=1}^{n} x_{s,i}\sigma_{ii}^2}{\sum_{i=1}^{n} x_{s,i}\sigma_{ii}^3} \quad (24)$$

The term $g_1(\sigma_{ii})$ is obtained from a self-consistent representation of the pressure p from the Clausius virial theorem and from the density derivative of the Helmholtz free energy[19,20]

$$g_1(\sigma_{ii};\zeta_3) = g_0^{HS}[\sigma_x;\zeta_x^{eff}] + (\lambda_{ii}^3 - 1)\frac{\partial g_0^{HS}[\sigma_x;\zeta_x^{eff}]}{\partial \zeta_x^{eff}}\left(\frac{\lambda_{ii}}{3}\frac{\partial \zeta_x^{eff}}{\partial \lambda_{ii}} - \zeta_3\frac{\partial \zeta_x^{eff}}{\partial \zeta_3}\right) \quad (25)$$

We should note that in the SAFT-HS approach[21] the attractive forces are described at the van der Waals level, and the hard-sphere contact value is used in the expression for the chain contribution.

Using standard thermodynamic relationships, other thermodynamic properties can be obtained from the Helmholtz free energy such as the chemical potential

$$\mu_i = \left(\frac{\partial A}{\partial N_i}\right)_{T,V,N_{j\neq i}} \quad (26)$$

and the compressibility factor

$$Z = \frac{pV}{NkT} = \sum_i^n \left(x_i\frac{\mu_i}{kT}\right) - \frac{A}{NkT} \quad (27)$$

These are the functions required for the determination of the critical and phase behavior of the mixture. The gas−liquid and liquid−liquid critical lines can be determined by equating the second and third derivatives of the Gibbs free energy with respect to the mole fraction to zero. Phase equilibria between phases I and II in mixtures requires that the temperature, pressure, and chemical potential of each component in each phase be equal[13]

$$T^{I} = T^{II}, \quad p^{I} = p^{II}, \quad \mu_i^{I} = \mu_i^{II} \quad (28)$$

These conditions are solved numerically using a simplex method.[33]

3. Results and Discussion

Theoretical phase diagrams for each perfluoro-(*n*)-alkane + (*n*)-alkane binary mixture are obtained within the SAFT-VR theory using a square-well model of variable attractive range and compared with the available experimental data. The parameters for each pure component are obtained by fitting to experimental data for the vapor pressure and saturated liquid density, from the critical to the triple point.[34] These optimized pure component parameters are then rescaled to the respective experimental critical points since our main interest is in the critical lines. The values of the parameters used in our study for the perfluoro-(*n*)-alkanes and (*n*)-alkanes are given in Tables 1 and 2, respectively. In Figure 1a we show the vapor pressures obtained with the SAFT-VR approach for methane through *n*-octane, and in Figure 1b the vapor pressures for perfluoromethane through perfluoro-*n*-butane, together with the corresponding experimental data.[34,35]

TABLE 1: Optimized Square-Well Intermolecular Potential Parameters for (*n*)-Alkanes[a]

substance	m	λ	σ (Å)	ϵ/k (K)	T_c^*	p_c^*
CH_4	1	1.444	4.069	157.4	0.1503	0.009 259
C_2H_6	1.33	1.449	4.233	224.8	0.1665	0.007 651
C_3H_8	1.67	1.452	4.363	249.3	0.1799	0.006 524
C_4H_{10}	2.0	1.501	4.395	243.1	0.1835	0.005 274
C_5H_{12}	2.33	1.505	4.475	252.7	0.1927	0.004 700
C_6H_{14}	2.67	1.552	4.479	236.6	0.1957	0.003 995
C_7H_{16}	3.0	1.563	4.529	237.3	0.2021	0.003 607
C_8H_{18}	3.33	1.574	4.564	236.5	0.2076	0.003 275

[a] m is the number of spherical segments in the model, λ the range parameter, σ the diameter of each segment, and ϵ the well depth. $T_c^* = kT_cb/\alpha$ and $p_c^* = p_cb^2/\alpha$ are the reduced critical temperature and pressure, where $\alpha = 4b\epsilon(\lambda^3 - 1)$ and $b = \pi\sigma^3/6$.

TABLE 2: Optimized Square-Well Intermolecular Potential Parameters for Perfluoro-(*n*)-alkanes[a]

substance	m	λ	σ (Å)	ϵ/k (K)	T_c^*	p_c^*
CF_4	1	1.287	5.237	254.0	0.1976	0.017 71
C_2F_6	1.37	1.339	5.133	268.6	0.1949	0.010 37
C_3F_8	1.74	1.359	5.092	281.7	0.2025	0.007 874
C_4F_{10}	2.11	1.406	5.056	267.9	0.2030	0.005 982

[a] m is the number of spherical segments in the model, λ the range parameter, σ the diameter of each segment, and ϵ the well depth. $T_c^* = kT_cb/\alpha$ and $p_c^* = p_cb^2/\alpha$ are the reduced critical temperature and pressure, where $\alpha = 4b\epsilon(\lambda^3 - 1)$ and $b = \pi\sigma^3/6$.

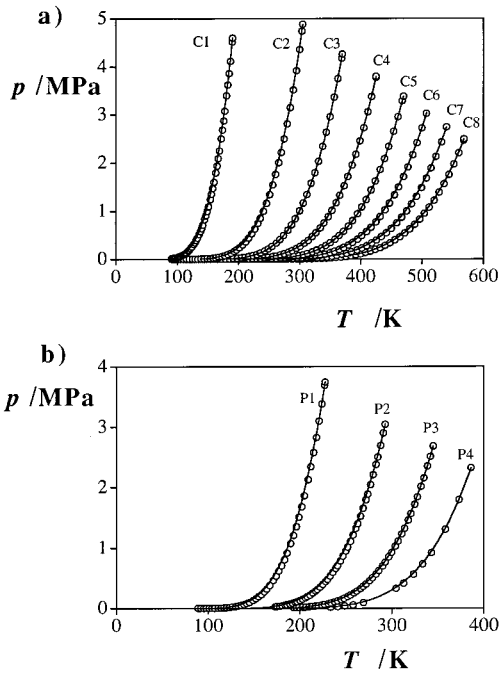

Figure 1. (a) Vapor pressure curves for methane through *n*-octane; (b) vapor pressures for perfluoromethane through perfluoro-*n*-butane. The circles represent the experimental data.[34,35] The continuous curves represent the SAFT-VR results obtained using parameters fitted to vapor pressure and saturated liquid density data, rescaled to the critical temperature and pressure of each pure component.

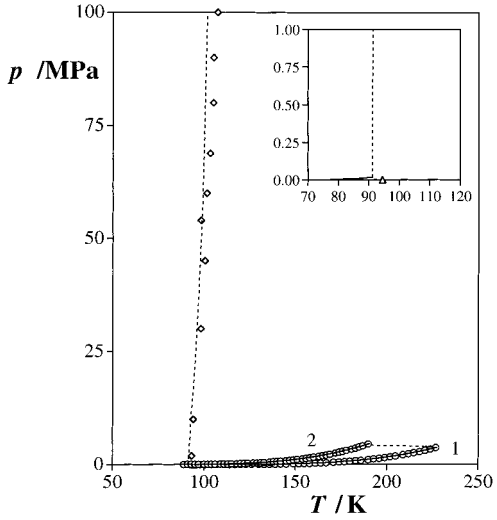

Figure 2. *pT* projection for perfluoromethane (1) + methane (2) compared with the SAFT-VR prediction. The circles represent the experimental values for the vapor pressures of the pure components,[34] the diamonds the liquid−liquid critical points,[36] and the triangle the UCEP.[37] The continuous curves represent the SAFT-VR vapor pressures for the pure components and the dashed curves the gas−liquid and liquid−liquid critical lines.

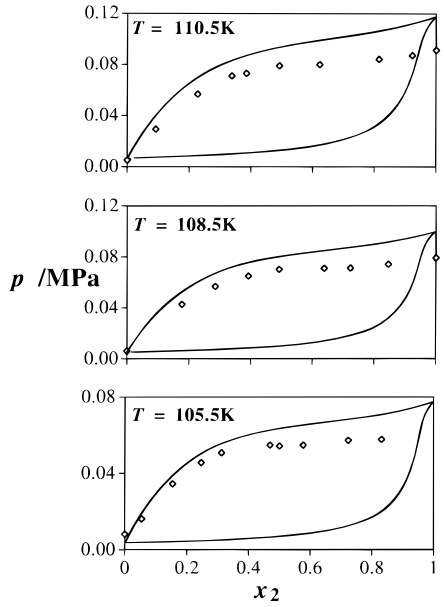

Figure 3. *px* slices at 110.5, 108.5, and 105.5 K for perfluoromethane (1) + methane (2) compared with SAFT-VR predictions. The diamonds correspond to the experimental data[40] and the continuous curves the theoretical predictions.

The study of phase equilibria in mixtures also requires the determination of a number of cross, or unlike, parameters. The following combining rules[13] were used to obtain the unlike size

$$\sigma_{12} = \frac{\sigma_1 + \sigma_2}{2} \tag{29}$$

and energy parameters

$$\epsilon_{12} = \xi(\epsilon_1\epsilon_2)^{1/2} \tag{30}$$

where eq 29 corresponds to the Lorentz rule and ξ in eq 30 describes the departure of the system from the Berthelot rule and the extensive regions of liquid−liquid immiscibility displayed by these mixtures. The unlike mean field energy ϵ_{12} is treated as an adjustable parameter that we optimize by changing ξ to give the best representation of the continuous liquid−liquid gas−liquid critical line in the perfluoromethane + *n*-butane system. The perfluoromethane + *n*-butane system was chosen to fit the correction parameter ξ since this system exhibits the change in phase behavior from type II to type III, displaying maxima and minima in the high-pressure critical line. This correction parameter is used in a transferable fashion for the other perfluoromethane + (*n*)-alkane systems, so eliminating the need for refitting. A value of $\xi = 0.9206$ is obtained by optimization. The unlike range parameter is obtained from the arithmetic mean of the pure component values as in previous papers[25,26]

$$\lambda_{ij} = \frac{\lambda_{ii}\sigma_{ii} + \lambda_{jj}\sigma_{jj}}{\sigma_{ii} + \sigma_{jj}} \tag{31}$$

The *pT* projection of the *pTx* surface for the perfluoromethane + methane system are presented in Figure 2. As discussed in the Introduction this system shows type II phase behavior with two distinct critical lines. As observed experimentally the gas−liquid critical line is a short almost straight line between the critical points of the two pure components,[36] and at lower temperatures we have the locus of UCSTs, which gradually increase with pressure. The literature value for the UCEP, most clearly seen in the inset of Figure 2, is 94.5 K,[37] with a predicted value of 91.3 K. However, given that we are fitting the unlike interaction parameter to the perfluoromethane + *n*-butane system we are achieving very good agreement between our theoretical predictions and the experimental data. In Figure 3 we present three constant temperature *px* slices as predicted with the SAFT-VR approach with the corresponding experimental data for the perfluoromethane + methane system. We reproduce the experimental data reasonably well, and it should be noted that at these temperatures we are just above the locus of UCST's and hence the dew point curve is quite flat. Since we are mainly interested in the behavior of the critical lines of the perfluoroalkane + *n*-alkane systems, we rescale the optimized parameters to the experimental critical points of the respective pure components; this gives a better representation curve near the critical point with a detriment to the saturated liquid densities, and hence in Figure 3 we overpredict the pure component pressure in the *px* slices compared to the experimental values.

When we look at the next member of the alkane homologous series with perfluoromethane, we achieve excellent agreement between SAFT-VR predictions and experimental results as seen in Figure 4. The line of UCSTs for perfluoromethane + ethane has shifted to higher temperatures and also extends to higher pressures with a positive slope. The predicted value for the UCEP is 153.8 K, compared with 150.1 K observed experimentally.[38] Figure 5 shows a constant pressure *Tx* slice for the perfluoromethane + ethane system compared with experimental points.[38] The solid curve represents the SAFT-VR prediction using MX1b mixing rule described earlier, and the dashed that of MX3b where the actual packing fraction of the system ζ_3 is used to obtain ζ_3^{eff} according to the mapping rule for pure components.[19,20] The MX3b mixing rule was used in a previous paper;[25] however, as can be seen from Figure 5 when studying systems that exhibit large regions of liquid−liquid immiscibility, we find inconsistencies in the description of the UCST when it is used. The MX1b mixing rule gives an excellent representation of both the vapor−liquid and liquid−liquid critical behavior

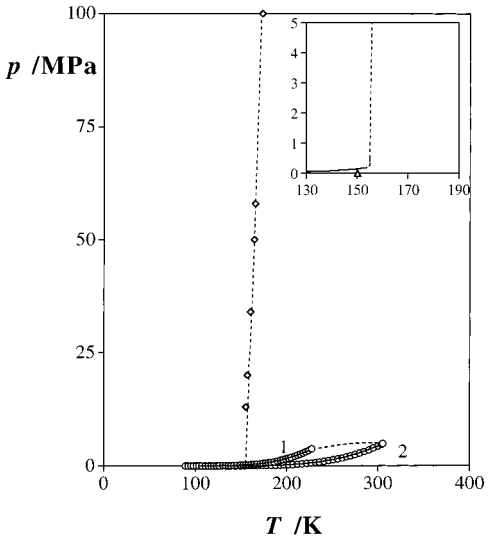

Figure 4. *pT* projection for perfluoromethane (1) + ethane (2) compared with the SAFT-VR predictions. The circles represent the experimental vapor pressure data for the pure components,[34] the diamonds the liquid−liquid critical points,[41] and the triangle the UCEP.[38] The continuous curves describe the SAFT-VR prediction for the vapor pressures and the dashed curves the critical lines.

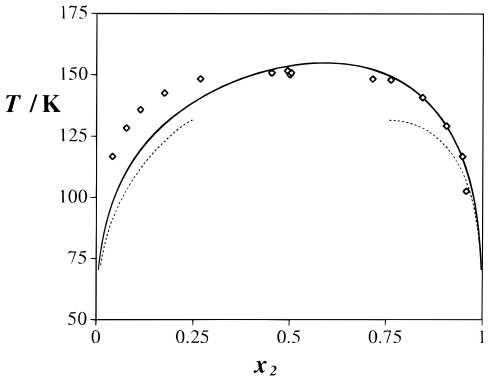

Figure 5. *Tx* liquid−liquid coexistence slice at 0.5 MPa for the perfluoromethane (1) + ethane (2) system. The diamonds correspond to the experimental data.[38] The continuous curve is the SAFT-VR prediction using mixing rule MX1b and the dashed line that for rule MX3b.

in binary mixtures of perfluoromethane + *n*-alkanes, as can be seen from the comparison in Figure 5. The theory, although slightly overpredicting the UCST,[17] describes the liquid−liquid coexistence curve very well.

For the perfluoromethane + propane binary mixture (Figure 6), we again accurately represent the fluid phase equilibria of this system albeit for the limited experimental data available. The line of UCSTs has shifted to higher temperature, indicating that the two components are becoming less miscible as the chain length of the *n*-alkane is increased. *Tx* slices for this system over a wide pressure range, from 10 to 200 MPa, are shown in Figure 7. The SAFT-VR approach predicts the liquid−liquid coexistence envelopes very well given the range of the experimental data and the flatness of the curves close to the liquid−liquid critical point.

The systems studied so far all display type II phase equilibria, but when the perfluoromethane + *n*-butane binary mixture is examined we observe type III phase behavior. This system is especially interesting to study as it is clearly intermediate between types II and III, still retaining the features of the liquid−liquid and gas−liquid critical lines. As discussed earlier we

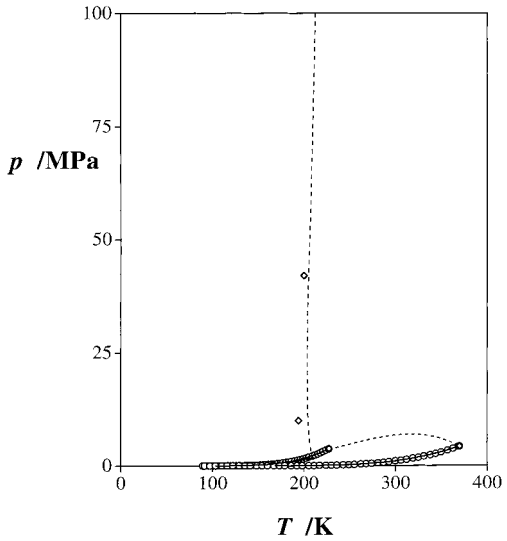

Figure 6. *pT* projection for perfluoromethane (1) + propane (2) compared with the SAFT-VR predictions. The circles represent the experimental vapor pressure data for the pure components[34] and the diamonds liquid−liquid critical points.[42] The continuous curves describe the SAFT-VR prediction for the vapor pressures and the dashed curves the critical lines.

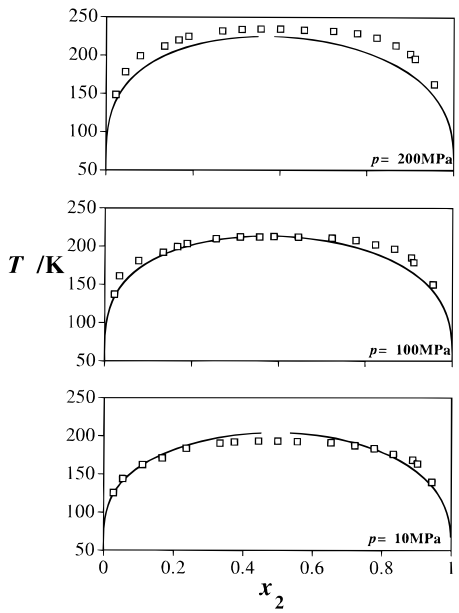

Figure 7. *Tx* slices at 10, 100, and 200 MPa for perfluoromethane (1) + propane (2). The squares correspond to the experimental data[42] and the continuous curves to the theoretical predictions obtained from SAFT-VR.

fit the unlike interaction parameter to this system in order to describe the pressure maximum and minimum of the continuous gas−liquid/liquid−liquid critical line. The dotted line in Figure 8 is the SAFT-HS prediction for the high-pressure critical line; a notable improvement is found with the SAFT-VR approach. The SAFT-VR prediction is remarkably accurate passing through a temperature minima at 231 K, compared with the experimental value of 236 K,[39] and extends to higher pressures with a positive slope resulting in gas−gas immiscibility of the second kind. Focusing on the inset of Figure 8, we can see the region close to the critical point of perfluoromethane more clearly. The solid curve is the predicted three-phase line, running from low temperatures and pressures to the UCEP, where it meets a short gas−liquid critical line. Given the

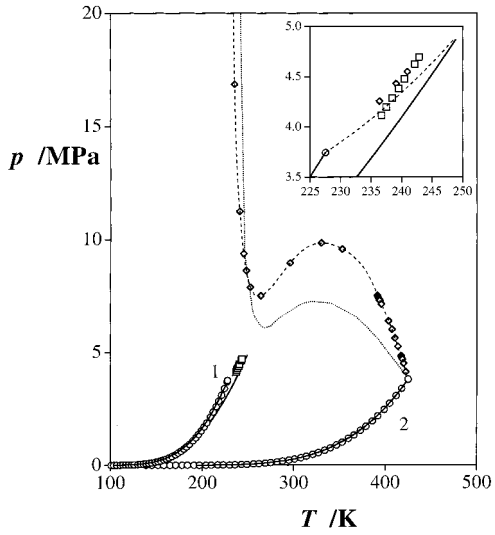

Figure 8. *pT* projection for perfluoromethane (1) + *n*-butane (2) compared with SAFT-VR predictions. The circles represent the experimental vapor pressure data,[34] the diamonds the gas−liquid and liquid−liquid critical points,[17,36] and the squares the three-phase line.[17] The continuous curves describe the SAFT-VR prediction for the vapor pressures and the three-phase line, and the dashed curve describes the critical lines. The dotted curve represents the SAFT-HS prediction.

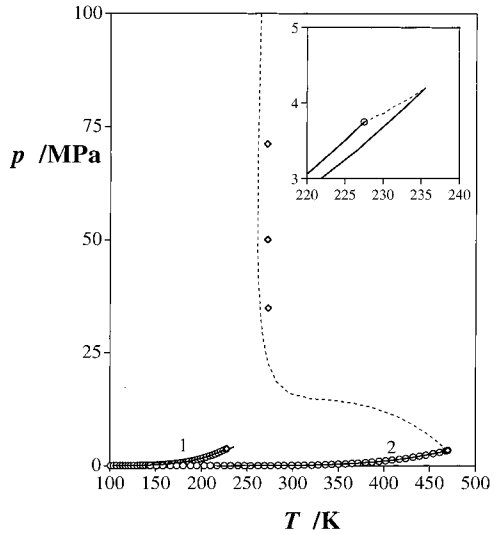

Figure 9. *pT* projection perfluoromethane (1) + *n*-pentane (2) compared with the SAFT-VR predictions. The circles represent the experimental vapor pressure data[34] and the diamonds the experimental liquid−liquid critical points.[36] The continuous curves represent the SAFT-VR vapor pressures for the pure components, and the dashed curves correspond to the critical lines.

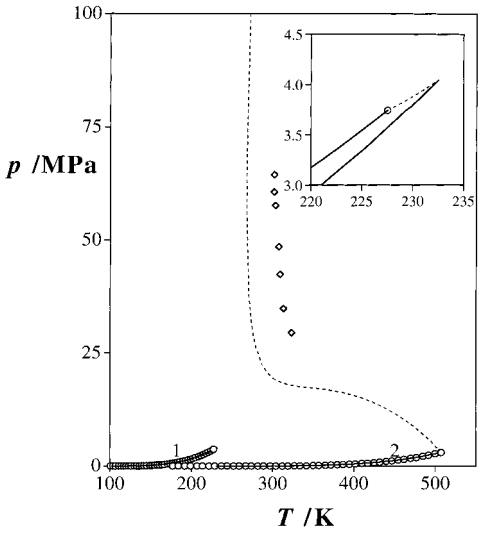

Figure 10. *pT* projection for perfluoromethane (1) + *n*-hexane (2) compared with the SAFT-VR predictions. The circles represent the experimental vapor pressure data[34] and the diamonds the liquid−liquid critical points.[36] The continuous curves represent the SAFT-VR vapor pressures for the pure components, and the dashed curves correspond to the critical lines.

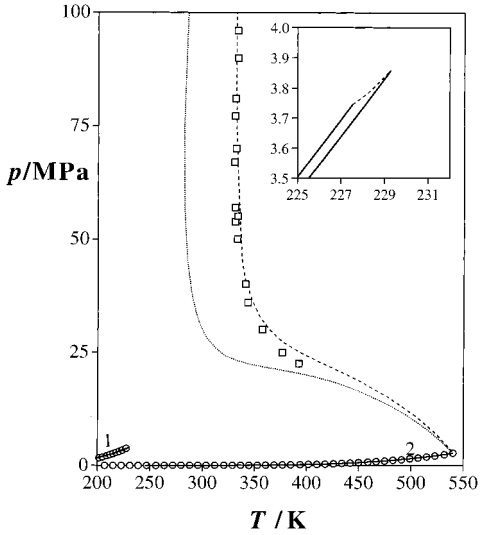

Figure 11. *pT* projection for perfluoromethane (1) + *n*-heptane (2) compared with the SAFT-VR predictions. The circles represent the experimental values for the vapor pressures of the pure components[34] and the triangles the gas−liquid and liquid−liquid critical points.[39] The continuous curves represent the SAFT-VR vapor pressures for the pure components, the dashed curve corresponds to the critical lines obtained with $\xi = 0.8948$, and the dotted curve that with $\xi = 0.9206$.

extremely small temperature range, the SAFT-VR approach describes this critical region reasonably accurately, only very slightly overestimating the UCEP; the experimental values are 242.89 K and 4.697 MPa,[17] and the predicted values 248.85 K and 4.869 MPa.

In Figure 9 we show the *pT* projection for the perfluoromethane + *n*-pentane system. Here, we clearly have a type III phase diagram with gas−gas immiscibility of the second kind at higher pressures than those shown, which is well-represented by the theoretical prediction. The quoted minimum in this high-pressure critical line is 271 K,[39] which compares favorably with the theoretical value of 261 K. For systems that are much larger than *n*-butane, which we used to obtain the ξ parameter, we observe a greater deviation between the experimental values and SAFT-VR predictions. The perfluoromethane + *n*-hexane predictions show a slight deviation from the experimental data, as seen in Figure 10, however the *n*-heptane mixture shows a more significant deviation of about 70 K. In order to study binary mixtures of longer chain length, we refitted the cross-interaction parameter to the high-pressure critical line, obtaining a ξ value of 0.8948, the results of which are shown by the dashed line in Figure 11. The high-pressure critical line passes through a temperature minimum, again indicating gas−gas immiscibility of the second kind, at 331.7 K,[39] which is in excellent agreement with the theoretical value of 331 K. When looking at the *px* slices for this system shown in Figure 12 at high temperatures we have two two-phase regions as a consequence of the temperature minimum. The high-pressure

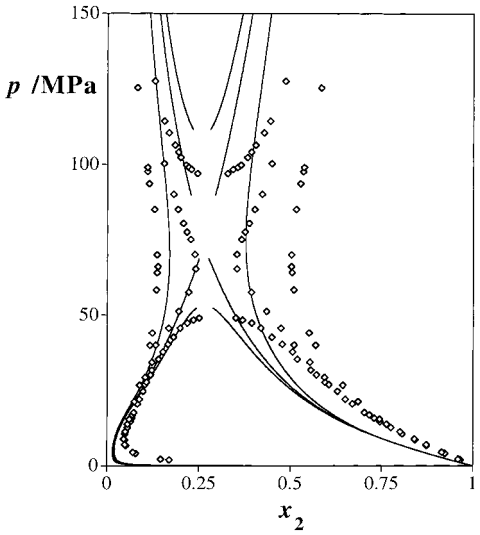

Figure 12. *px* slices at 333.15 K, 330.15 K, and 323.15 K (from the inner to the outer curves) for perfluoromethane (1) + *n*-heptane (2) compared with the SAFT-VR prediction. The solid curves represent the theoretical coexistence curves and the diamonds the experimental data.[16]

region can be assigned to a liquid−liquid and the low-pressure to a gas−liquid coexistence. As the temperature decreases, the two phase regions move toward each other until they merge at the point of double contact, below which there is only a single two-phase region. This can be seen very clearly in Figure 12 where we compare SAFT-VR predictions with experimental data at three constant temperatures. The SAFT-VR approach reproduces the experimental data well, the theoretical slices being slightly narrower than those observed experimentally.

The critical lines for perfluoromethane + methane through perfluoromethane + *n*-hexane are summarized in Figure 13. We can clearly see type II phase behavior for the systems up to and including propane, where the liquid−liquid critical line is very close to the critical point of perfluoromethane. For the *n*-butane system, the liquid−liquid critical line has passed the critical point of perfluoromethane and merged with the gas−liquid critical line to give us type III phase behavior. It is important to note that we adjust the cross-interaction parameter ξ to describe accurately the maximum and minimum in the critical pressure for the perfluoromethane + *n*-butane system, and then transfer the ξ parameter to the other binary systems up to *n*-hexane. The systems studied beyond *n*-butane describe more typical type III phase behavior, with the high-pressure critical line passing through a temperature minimum before extending to higher pressures with a positive slope corresponding to gas−gas immiscibility of the second kind. This minimum shifts to higher temperatures with increasing chain length of the *n*-alkane, indicating a decrease in the mutual solubility of the two components. Using this transferable parameter approach we reproduce the experimental data extremely well, seeing only a slight deviation between theory and experiment as chain length increases.

We have also studied a number of symmetrical perfluoroalkane + (*n*)-alkane binary systems. The phase diagrams of such mixtures are characterized by type II behavior with the addition of heteroazeotropy, which arises because the three-phase line lies above the vapor pressure curves of both pure components. The *pT* projection of the *pTx* surface for the perfluorobutane + *n*-butane system is shown in Figure 14; the azeotropic line can be seen more clearly at low temperatures and pressures where there are a few experimental data points, shown in the inset of

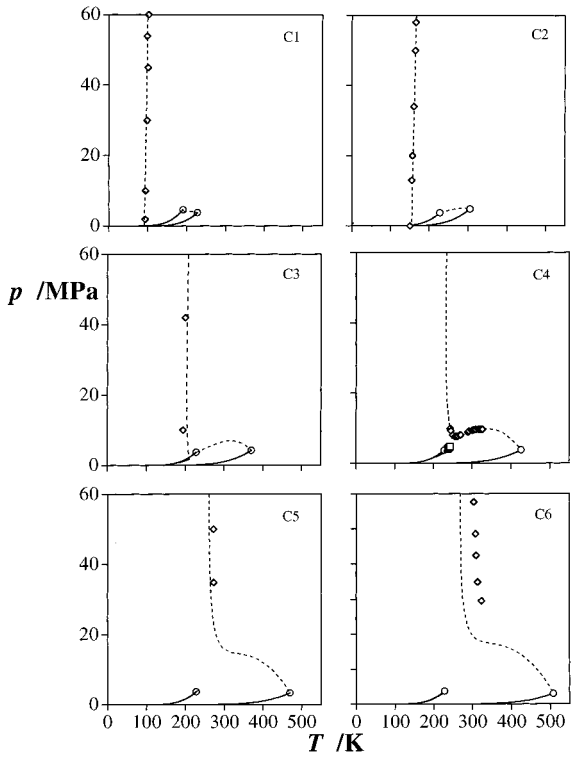

Figure 13. *pT* projections of the perfluoromethane (1) + *n*-alkane (2) systems compared with the SAFT-VR predictions. The diamonds represent the experimental data, the solid curves represent the calculated vapor pressure curves, and the dashed curves describe the critical lines.

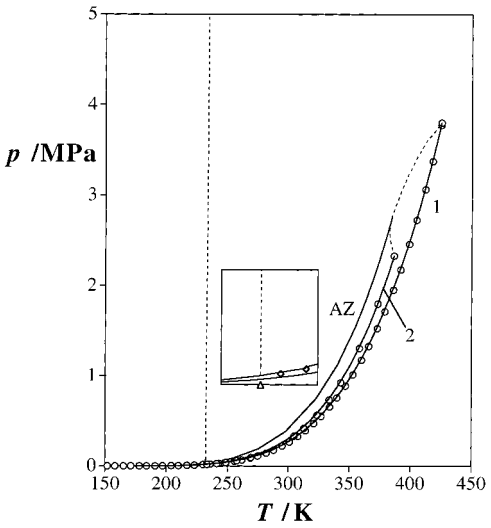

Figure 14. *pT* projection for butane (1) + perfluorobutane (2) compared with the SAFT-VR predictions. The circles represent experimental vapor pressure data[34,35] and the triangle the UCST.[4] The solid lines represent the SAFT-VR predictions for the vapor pressure curves, the continuous curve labeled AZ represents the calculated azeotropic curve, and the dashed lines represent the gas−liquid and liquid−liquid critical lines.

the figure. The triangle represents the UCST (232 K) to which we fitted the unlike interaction parameter obtaining a value of $\xi = 0.9234$, which is very similar to $\xi = 0.9206$, which we obtained for the unsymmetrical systems. The SAFT-VR approach provides a good representation of the phase diagram for this system; unfortunately, there is limited experimental data available, although there is good agreement with the azeotropic

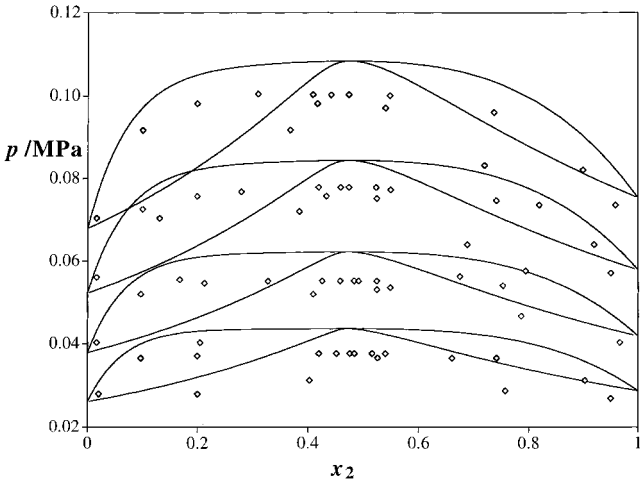

Figure 15. *px* slices at 259.95 K, 253.62 K, 246.35 K, and 238.45 K for butane (1) + perfluorobutane (2) compared with SAFT-VR predictions. The diamonds describe the experimental data[35] and the solid curves the predictions.

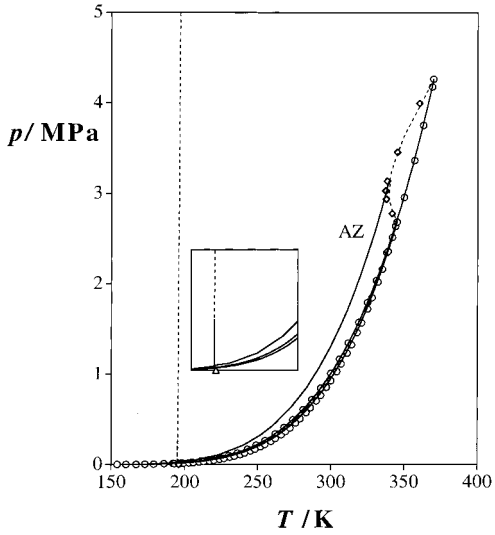

Figure 16. *pT* projection for propane (1) + perfluoropropane (2) compared with the SAFT-VR predictions. The circles correspond to experimental vapor pressure data,[34] the triangle corresponds to the UCEP,[43] the diamonds correspond to points on the gas−liquid critical line,[31] the solid curves correspond to the calculated vapor pressure and three-phase lines, and the dashed curves correspond to the critical lines.

points. Four constant temperature *px* slices corresponding to 238.45, 246.35, 253.62, and 259.95 K are shown in Figure 15. The curves are very flat, being just above the UCST at 238.45 K, with the slices getting broader as the temperature rises. The theoretical prediction of the vapor−liquid coexistence is good given that we have fitted the parameters to the liquid−liquid coexistence region. The *pT* projection for perfluoropropane + propane was determined using the ξ parameter obtained from the symmetrical butane system, so eliminating the need for refitting. In Figure 16 we present the theoretical phase diagram for this system and the available experimental data for the gas−liquid critical line, which are in very good agreement. Experimentally the UCST is quoted at 196 K, which compares well with a theoretical value of 195 K, especially when we remember we are using ξ obtained from the perfluorobutane + butane system. Finally, in Figure 17, we present three constant temperature *px* slices for the symmetrical perfluoropropane + propane system compared with SAFT-VR predictions. Again

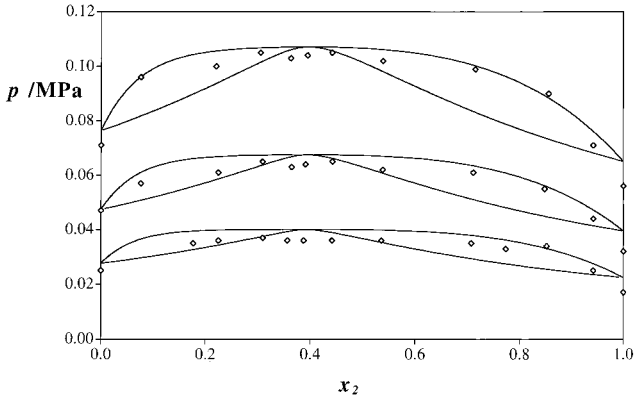

Figure 17. *px* slices at 223.5 K, 213.6 K, and 203.5 K for propane (1) + perfluoropropane (2) compared with SAFT-VR predictions. The continuous curves represent the theoretical predictions and the diamonds the experimental data.[43]

the slice at 203.5 K is just above the UCST and is therefore very narrow and flat, this effect decreasing as temperature increases.

4. Conclusion

We have used SAFT-VR, a version of the SAFT approach for potentials of variable attractive range, to describe the phase behavior of perfluoro-(*n*)-alkane + (*n*)-alkane systems. The parameters for the pure components are rescaled to the experimental critical points as we are concentrating on high-pressure phase behavior. Although we lose some accuracy on the vapor pressure curves, fitting to the critical point gives a better representation of the critical lines. The ξ parameter is obtained from a fit to a single binary mixture and used in the calculation of the unlike interaction for the other systems of interest. Using our parameters in this transferable fashion we avoid the need for refitting when studying a new system and still obtain a good description of the phase equilibrium for all systems studied, seeing only a slight deviation between theory and experiment for longer chain lengths. Since we are interested in the high-pressure behavior of the systems studied, mixing rule MX1b was used to avoid any inconsistencies in the critical region. MX3b would provide a accurate description of vapor−liquid equilibria but is not appropriate for critical behavior.

Acknowledgment. C.M. thanks Sheffield University for the award of a UGC Scholarship, A.G. thanks Sheffield University and ICI Chemicals and Polymers for a Roberts-Boucher Scholarship, and A.G.-V. thanks the Engineering and Physical Sciences Research Council (EPSRC) for funding a Research Fellowship. A.G.-V. was also funded by the ICI Strategic Research Fund as a Senior Research Fellow. We also acknowledge support from the European Commission, the Royal Society, and the Computational and ROPA Initiatives of the EPSRC for the provision of computer hardware.

References and Notes

(1) Hildebrand, J. H.; Scott, R. L. *Solubility of Nonelectrolytes*, 3rd ed.; Reinhold Publishing Corp.: New York, 1950.
(2) Scott, R. L. *J. Am. Chem. Soc.* **1948**, *70*, 4090.
(3) Hildebrand, J. H.; Fisher, B. B.; Benesi, H. A. *J. Am. Chem. Soc.* **1950**, *72*, 4348.
(4) Simons, J. H.; Mausteller, J. W. *J. Chem. Phys.* **1952**, *20*, 1516.
(5) Simons, J. H.; Dunlap, R. D. *J. Chem. Phys.* **1950**, *18*, 335.
(6) Hildebrand, J. H. *J. Chem. Phys.* **1950**, *18*, 1337.
(7) Dunlap, R. D. *J. Chem. Phys.* **1953**, *21*, 1293.
(8) Reed, T. M. *J. Phys. Chem.* **1955**, *59*, 425.
(9) Reed, T. M. *J. Phys. Chem.* **1959**, *63*, 1798.

(10) Rowlinson, J. S. *Liquids and Liquid Mixtures*, 2nd ed.; Butterworth Scientific: London, 1969.
(11) Dantzler Siebert, E. M.; Knobler, C. M. *J. Phys. Chem.* **1971**, *75*, 3863.
(12) Scott, R. L.; van Konynenburg, P. H. *Discuss. Faraday Soc.* **1970**, *49*, 87. van Konynenburg, P. H.; Scott, R. L. *Philos. Trans. R. Soc. London A* **1980**, *298*, 495.
(13) Rowlinson, J. S.; Swinton, F. L. *Liquids and Liquid Mixtures*, 3rd ed.; Butterworth Scientific: London, 1982.
(14) Pass, R.; Schneider, G. M. *J. Chem. Thermodyn.* **1979**, *11*, 267. Peter, K. H.; Pass, R.; Schneider, G. M. *J. Chem. Thermodyn.* **1976**, *8*, 731. Jeschke, P.; Schneider, G. M. *J. Chem. Thermodyn.* **1982**, *14*, 547. Wirths, M.; Schneider, G. M. *Fluid Phase Equilib.* **1985**, *21*, 257.
(15) Mukherjee, A. Ph.D. Thesis, Imperial College, London, 1978.
(16) Mendonça, J. M. M. Ph.D. Thesis, Imperial College, London, 1979.
(17) De Loos, TH. W.; Poot, W.; De Swaan Arons, J. *J. Chem. Thermodyn.* **1989**, *21*, 113.
(18) Deiters, U. K. Habilitationsscrift, University of Bochum, Bochum, 1985; *Chem. Eng. Sci.* **1981**, *36*, 1139.
(19) Gil-Villegas, A.; Galindo, A.; Whitehead, P. J.; Mills, S. J.; Jackson, G.; Burgess, A. N. *J. Chem. Phys.* **1997**, *106*, 4168.
(20) Galindo, A.; Davies, L. A.; Gil-Villegas, A.; Jackson, G. *Mol. Phys.* **1998**, *93*, 241.
(21) Galindo, A.; Whitehead, P. J.; Jackson, G.; Burgess, A. N. *J. Phys. Chem.* **1996**, *100*, 6781.
(22) Jackson, G.; Gubbins, K. E. *Pure Appl. Chem.* **1989**, *61*, 1021.
(23) Archer, A. L.; Amos, M. D.; Jackson, G.; McLure, I. A. *Int. J. Thermophys.* **1996**, *17*, 201.
(24) Clements, P. J.; Zafar, S.; Galindo, A.; Jackson, G.; McLure, I. A. *J. Chem. Soc., Faraday Trans.* **1997**, *93*, 1331.
(25) McCabe, C.; Galindo, A.; Gil-Villegas, A.; Jackson, G. *Int. J. Thermophys.* **1998**, in press.
(26) McCabe, C.; Gil-Villegas, A.; Jackson, G. *J. Phys. Chem. B* **1998**, *102*, 4183.
(27) Hansen, J. P.; McDonald, I. R. *Theory of Simple Liquids*, 2nd ed.; Academic Press: New York, 1986.
(28) Leonard, P. J.; Henderson, D.; Barker, J. A. *Trans. Faraday Soc.* **1970**, *66*, 2439.
(29) Boublík, T. *J. Chem. Phys.* **1970**, *53*, 471.
(30) Mansoori, G. A.; Carnahan, N. F.; Starling, K. E.; Leland, T. W. *J. Chem. Phys.* **1971**, *54*, 1523.
(31) Carnahan, N. F.; Starling, K. E. *J. Chem. Phys.* **1969**, *51*, 635.
(32) Hicks, C. P.; Young, C. L. *Chem. Rev.* **1975**, *75*, 119.
(33) Press, W. H.; Teukolsky, S. A.; Vetterling, W. T.; Flannery, B. P. *Numerical Recipes in Fortran*, 1st ed.; Cambridge University Press: Cambridge, 1986.
(34) Smith, B. D.; Srivastava, R. *Thermodynamic Data for Pure Compounds*; Elsevier: London, 1986.
(35) Brown, J. A.; Mears, W. H. *J. Phys. Chem.* **1958**, *62*, 960.
(36) Paas, R.; Schneider, G. M. *J. Chem. Thermodyn.* **1979**, *11*, 1979.
(37) Croll, I. M.; Scott, R. L. *J. Phys. Chem.* **1958**, *62*, 954.
(38) Croll, I. M.; Scott, R. L. *J. Phys. Chem.* **1964**, *68*, 3853.
(39) Wirths, M.; Schneider, G. M. *Fluid Phase Equilib.* **1985**, *21*, 257.
(40) Thorpe, N.; Scott, R. L. *J. Phys. Chem.* **1956**, *60*, 670.
(41) Peter, K. H.; Pass, R.; Schneider, G. M. *J. Chem. Thermodyn.* **1976**, *8*, 731.
(42) Jeschke, P.; Schneider, G. M. *J. Chem. Thermodyn.* **1982**, *14*, 547.
(43) Gilmour, J. B.; Zwicker, J. O.; Katz, J.; Scott, R. L. *J. Phys. Chem.* **1967**, *71*, 3529.